



HARMONICa: HARMONIZING TRAINING AND INFERENCE FOR BETTER FEATURE CACHE IN DIFFUSION TRANSFORMER ACCELERATION

Yushi Huang^{1*}, Zining Wang^{1,2*}, Ruihao Gong^{1,2†}, Jing Liu³, Xinjie Zhang⁴, Jinyang Guo², Xianglong Liu², Jun Zhang^{4†}

¹SenseTime Research ²Beihang University ³Monash University ⁴HKUST
 {huangyushi, ziningwang, gongruihao}@sensetime.com, liujing_95@outlook.com,
 xinjie.zhang@connect.ust.hk, {jinyangguo, xlliu}@buaa.edu.cn,
 eejzhang@ust.hk

"A tranquil forest clearing bathed in soft, magical light, filled with fairies dancing among the flowers. The pastel chalk drawing style gives the image a delicate, almost ethereal quality, with soft, smudged edges and gentle, powdery colors blending seamlessly."



(a) PIXART- Σ w/o feature cache



(b) HarmoniCa ($\times 1.68$)

Figure 1: High-resolution 2048×2048 images generated using PIXART- Σ (Chen et al., 2024a) with a 20-step DPM-Solver++ sampler (Lu et al., 2022b). Our proposed feature cache framework achieves a substantial $\times 1.68$ speedup. More visualization results can be found in Sec. K.

ABSTRACT

Diffusion Transformers (DiTs) have gained prominence for outstanding scalability and extraordinary performance in generative tasks. However, their considerable inference costs impede practical deployment. The feature cache mechanism, which involves storing and retrieving redundant computations across timesteps, holds promise for reducing per-step inference time in diffusion models. Most existing caching methods for DiT are manually designed. Although the learning-based approach attempts to optimize strategies adaptively, it suffers from discrepancies between training and inference, which hampers both the performance and acceleration ratio. Upon detailed analysis, we pinpoint that these discrepancies primarily stem from two aspects: (1) *Prior Timestep Disregard*, where training ignores the effect of cache usage at earlier timesteps, and (2) *Objective Mismatch*, where the training target (align predicted noise in each timestep) deviates from

*Equal contribution; work completed during internships at SenseTime Research.

†Corresponding authors.

the goal of inference (generate the high-quality image). To alleviate these discrepancies, we propose **HarmoniCa**, a novel method that **Harmonizes** training and inference with a novel learning-based **Caching** framework built upon *Step-Wise Denoising Training* (SDT) and *Image Error Proxy-Guided Objective* (IEPO). Compared to the traditional training paradigm, the newly proposed SDT maintains the continuity of the denoising process, enabling the model to leverage information from prior timesteps during training, similar to the way it operates during inference. Furthermore, we design IEPO, which integrates an efficient proxy mechanism to approximate the final image error caused by reusing the cached feature. Therefore, IEPO helps balance final image quality and cache utilization, resolving the issue of training that only considers the impact of cache usage on the predicted output at each timestep. Extensive experiments on class-conditional and text-to-image (T2I) tasks for 7 models and 4 samplers with resolutions ranging from 256×256 to 2048×2048 demonstrate the exceptional performance and speedup capabilities of our HarmoniCa. For example, HarmoniCa is the first feature cache method applied to the 20-step PIXART- α 1024×1024 that achieves over $1.5 \times$ speedup in latency with an improved FID compared to the non-accelerated model. Remarkably, HarmoniCa requires no image data during training and reduces about 25% of training time compared to the existing learning-based approach.

1 INTRODUCTION

Diffusion models (Ho et al., 2020; Dhariwal & Nichol, 2021) have recently gained increasing popularity in a variety of generative tasks, such as image (Saharia et al., 2022; Esser et al., 2024) and video generation (Blattmann et al., 2023; Ma et al., 2024a), due to their ability to produce diverse and high-quality samples. Among different backbones, Diffusion Transformers (DiTs) (Peebles & Xie, 2023) stand out for offering exceptional scalability. However, the extensive parameter size and multi-round denoising nature of diffusion models bring tremendous computational overhead during inference, limiting their practical applications. For instance, generating one 2048×2048 resolution image using PixArt- Σ (Chen et al., 2024a) with 0.6B parameters and 25 denoising rounds can take up to 14 seconds on a single NVIDIA H800 80GB GPU, which is unacceptable.

To accelerate the generation process of diffusion models, previous methods are developed from two perspectives: reducing the number of sampling steps (Liu et al., 2022; Song et al., 2020b) and decreasing the network complexity in noise prediction of each step (Fang et al., 2023; He et al., 2024). Recently, a new branch of research (Selvaraju et al., 2024; Yuan et al., 2024; Chen et al., 2024b) has started to focus on accelerating sampling time per step by the feature cache mechanism. This technique takes advantage of the repetitive computations across timesteps in diffusion models, allowing previously computed features to be cached and reused in later steps. Nevertheless, most existing methods are either tailored to the U-Net architecture (Ma et al., 2024c; Wimbauer et al., 2024) or develop their strategy based on empirical observations (Chen et al., 2024b; Selvaraju et al., 2024), and there is a lack of adaptive and systematic approaches for DiT models. Learning-to-Cache (Ma et al., 2024b) introduces a learnable router to guide the cache scheme for DiT models. However, this method induces discrepancies between training and inference, which always leads to distortion build-up (Ning et al., 2023; Li et al., 2024; Ning et al., 2024). The discrepancies arise from two main factors: (1) *Prior Timestep Disregard*: During training, the model directly samples a timestep and employs the training images manually added noise akin to DDPM (Hu et al., 2021), ignoring the impact of the feature cache mechanism from earlier steps, which differs from the inference process. (2) *Objective Mismatch*: The training objective minimizes noise prediction error of each timestep, while the inference goal aims for high-quality final images, causing a misalignment in objectives. We believe these inconsistencies hinder effective and efficient router learning.

To alleviate the above discrepancies effectively, we present harmonizing training and inference with HarmoniCa, a novel cache learning framework featuring a unique training paradigm and a distinct learning objective. Specifically, to mitigate the first disparity, we design *Step-Wise Denoising Training* (SDT), which aligns the training process with the full denoising trajectory of inference using a student-teacher model setup. The student utilizes the cache while the teacher does not, effectively mimicking the teacher’s outputs across all continuous timesteps. This approach maintains the reuse and update of the cache at earlier timesteps, similar to inference. Additionally, to address the mis-

alignment in optimization goals, we introduce the *Image Error Proxy-Guided Objective* (IEPO), which leverages a proxy to approximate the final image error and reduces the significant costs of directly utilizing the error to supervise training. This objective helps SDT efficiently balance cache usage and image quality. By combining SDT and IEPO, extensive experiments for text-to-image (T2I) and class-conditioned generation tasks show the promising performance and speedup ratio of HarmoniCa, e.g., a $\times 1.51$ speedup and even a lower FID (Nash et al., 2021) for PIXART- α 1024×1024 (Chen et al., 2023). In addition, HarmoniCa eliminates the requirement of training with a large amount of image data and reduces about 25% training time compared to the existing learning-based method (Ma et al., 2024b), further enhancing its applicability.

Our contributions are summarized as follows:

- We uncover two discrepancies between training and inference in the existing learning-based feature cache method: (1) *Prior Timestep Disregard*, indicating that the training process overlooks the influence of preceding timesteps, which is inconsistent with the inference process. (2) *Objective Mismatch*, minimizing intermediate outputs error, instead of the final image error. These discrepancies prevent the method from further performance and acceleration improvements.
- We propose a novel framework called HarmoniCa to alleviate the discovered discrepancies by: (1) *Step-Wise Denoising Training* (SDT), which addresses the first discrepancy by capturing the complete denoising trajectory, ensuring that the model learns to consider the impact of earlier timesteps. (2) *Image Error Proxy-Guided Optimization Objective* (IEPO), which mitigates the second discrepancy by using a proxy for the final image error, and thereby targets aligning the training objective with the inference.
- Extensive experiments on NVIDIA H800 80GB GPUs for DiT-XL/2, PIXART- α , and PIXART- Σ series—encompassing 7 models, 4 samplers, and 4 resolutions—proves the substantial efficacy and universality of HarmoniCa. For instance, it outperforms previous state-of-the-art (SOTA) by a 6.74 IS increase and 1.24 FID decrease with a higher speedup ratio on DiT-XL/2 256×256 . Notably, our image-free framework with much lower training costs exhibits superior efficiency and applicability than the current learning-based method.

2 RELATED WORK

Diffusion models. Diffusion models, initially conceptualized with the U-Net architecture (Ronneberger et al., 2015), have achieved satisfactory performance in image (Rombach et al., 2022; Podell et al., 2023) and video generation (Ho et al., 2022). Despite their success, U-Net models struggle with modeling long-range dependencies in complex, high-dimensional data. In response, the Diffusion Transformer (DiT) (Peebles & Xie, 2023; Chen et al., 2023; 2024a) is introduced, leveraging the inherent scalability of Transformers to efficiently enhance model capacities and handle more complex tasks with improved performance.

Efficient diffusion. Diverse methods have been proposed to tackle the poor real-time performance of diffusion models. These techniques fall into two main categories: reducing the number of sampling steps and decreasing the computational load per denoising step. In the first category, several works utilize distillation (Salimans & Ho, 2022; Luhman & Luhman, 2021) to obtain reduced sampling iterations. Furthermore, this category encompasses advanced techniques such as implicit samplers (Kong & Ping, 2021; Song et al., 2020a; Zhang et al., 2022) and specialized differential equation (DE) solvers. These solvers tackle both stochastic differential equations (SDE) (Song et al., 2020b; Jolicoeur-Martineau et al., 2021) and ordinary differential equations (ODE) (Lu et al., 2022a; Liu et al., 2022; Zhang & Chen, 2022), addressing diverse aspects of diffusion model optimization. In contrast, the second category mainly focuses on model compression. It leverages techniques like pruning (Fang et al., 2023; Zhang et al., 2024; Wang et al., 2024b) and quantization (Shang et al., 2023; Huang et al., 2024; He et al., 2024) to reduce the workload in a static way. Additionally, dynamic inference compression is also being explored (Liu et al., 2023; Pan et al., 2024), where different models are employed at varying steps of the process. In this work, we focus on the urgently needed DiT acceleration through feature cache, a method distinct from the above-discussed ones.

Feature cache. Due to the high similarity between activations (Li et al., 2023b; Wimbauer et al., 2024) across continuous denoising steps in diffusion models, recent studies (Ma et al., 2024c; Wimbauer et al., 2024; Li et al., 2023a) have explored caching these features for reuse in subsequent steps

to avoid redundant computations. Notably, their strategies rely heavily on the specialized structure of U-Net, *e.g.*, up-sampling blocks¹ or SpatialTransformer blocks². Besides, FORA (Selvaraju et al., 2024) and Δ -DiT (Chen et al., 2024b) further apply the feature cache mechanism to DiT. However, both methods select the cache position and lifespan in a handcrafted way. Learning-to-Cache (Ma et al., 2024b) introduces a learnable cache scheme but fails to harmonize training and inference. In this work, we design a new training framework, to alleviate the discrepancies between the training and inference, which further enhances the performance and acceleration ratio for DiT.

3 PRELIMILARIES

Cache granularity. The noise estimation network of DiT (Peebles & Xie, 2023) is built on the Transformer block (Vaswani, 2017), which is composed of an Attention block and a feed-forward network (FFN). Each Attention block and FFN is wrapped up in a residual connection (He et al., 2016). For convenience, we sequentially denote these Attention blocks and FFNs without residual connections as $\{b_0, b_1, \dots, b_{N-1}\}$, where N is their total amount. Following Ma et al. (2024b), we store the output of b_i in cache as c_i . The cache, once completely filled, is represented as follows:

$$\text{cache} = [c_0, c_1, \dots, c_{N-1}]. \quad (1)$$

Cache router. The cache scheme for DiT can be formulated with a pre-defined threshold τ ($0 \leq \tau < 1$) and a customized router matrix:

$$\text{Router} = [r_{t,i}]_{1 \leq t \leq T, 0 \leq i \leq N-1} \in \mathbb{R}^{T \times N}, \quad (2)$$

where $0 < r_{t,i} \leq 1$ and T is the maximum denoising step. At timestep t during inference, the residual corresponding to b_i is fused with o_i defined as follows:

$$o_i = \begin{cases} b_i(\mathbf{h}_i, \mathbf{cs}), & r_{t,i} > \tau \\ c_i, & r_{t,i} \leq \tau \end{cases}, \quad (3)$$

where \mathbf{h}_i is the image feature and \mathbf{cs} represents the conditional inputs³. Specifically, $r_{t,i} > \tau$ indicates computing $b_i(\mathbf{h}_i, \mathbf{cs})$ as o_i . This computed output also replaces c_i in the cache. Otherwise, the model loads c_i from cache without computation. Here we present a naive example of the cache scheme as depicted in Fig. 2. To be noted, $\text{Router}_{T,:}$ is set to $[1]_{1 \times N}$ by default to pre-fill the empty cache.

Cache usage ratio (CUR). In addition, we define cache usage ratio (CUR) formulated as $\frac{\sum_{t=1}^{t=T} \sum_{i=0}^{N-1} \mathbb{I}_{r_{t,i} \leq \tau}}{N \times T}$ in this paper to represent the reduced computation by reusing cached features. For instance, CUR is roughly equal to 33.33% in Fig. 2.

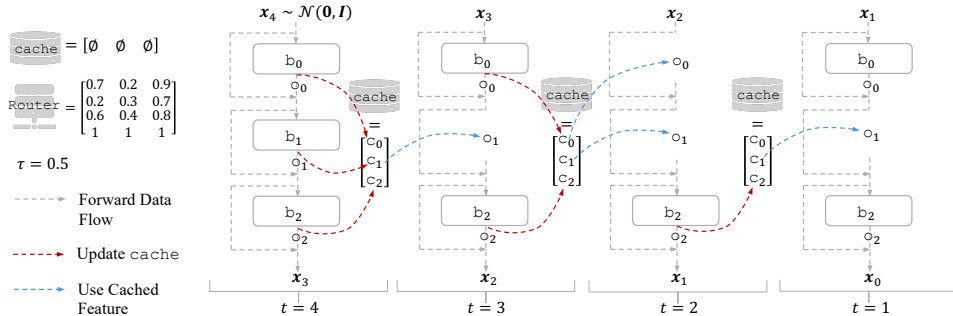


Figure 2: Generation process from a random Gaussian noise x_4 to an image x_0 using feature cache ($T = 4, N = 3$). We omit the sampler (Ho et al., 2020; Song et al., 2020a) and conditional inputs.

¹<https://github.com/CompVis/stable-diffusion/blob/main/ldm/modules/diffusionmodules/openaimodel.py#L626>

²<https://github.com/CompVis/stable-diffusion/blob/main/ldm/modules/attention.py#L218>

³For example, \mathbf{cs} represents the time condition and textual condition for text-to-image (T2I) generation.

4 HARMONICA

In this section, we first observe that the existing learning-based feature cache strategy shows discrepancies between the training and inference (Sec. 4.1). Then, we propose a framework named **HarmoniCa** to **Harmonize** them for better feature **Cache** (Sec. 4.2). Finally, our HarmoniCa shows higher efficiency and better applicability than the previous training-based method (Sec. 4.3).

4.1 DISCREPANCY BETWEEN TRAINING AND INFERENCE

Revealing previous approaches for DiT, most of them (Selvaraju et al., 2024; Chen et al., 2024b) manually set the value of the Router in a heuristic way. To be adaptive, Learning-to-Cache (Ma et al., 2024b) employs a learnable Router⁴. However, we have identified two discrepancies between its training and inference phases in the following.

Prior timestep disregard. As illustrated in Fig. 2, the inference process employing feature cache at timestep t is subject to the prior timesteps. For example, at timestep $t = 1$, the input x_1 has the error induced by reusing the cached features c_0 and c_1 at preceding timestep $t = 2$. Furthermore, reusing and updating features at earlier timesteps also shape the contents of the current cache.

However, Learning-to-Cache is unaffected by prior denoising steps during training. Specifically, for each training iteration, as depicted in Fig. 3 (a), it first uniformly samples a timestep t akin to DDPM (Ho et al., 2020). It then pre-fills an empty cache at t and proceeds to train Router $_{t-1,:}$ at subsequent timestep $t - 1$, without being influenced by the feature cache mechanism from timestep T to $t + 1$.

Objective mismatch. Moreover, we also find that Learning-to-Cache (Ma et al., 2024b) solely focuses on the predicted noise at each denoising step during training. It leverages the following learning objective at timestep t :

$$\mathcal{L}_{LTC}^{(t)} = \mathcal{L}_{MSE}^{(t)} + \beta \sum_{i=0}^{N-1} r_{t,i}, \tag{4}$$

where β is a coefficient for the regularization term of the Router $_{t,:}$, and $\mathcal{L}_{MSE}^{(t)}$ represents the Mean Square Error (MSE) between the predicted noise of the DiT with and without reusing cached features at t .

In contrast, the target during inference is to generate the high-quality image x_0 , which also leads to a discrepancy of objective.

4.2 HARMONIZING TRAINING AND INFERENCE

Existing studies (Ning et al., 2023; Li et al., 2024; Ning et al., 2024) on diffusion models show that discrepancies between training and inference phases can lead to error accumulation (Arora et al., 2022; Schmidt, 2019) and results in performance degradation. Therefore, we **Harmonize** training and inference with a new learning-based **Caching** framework called **HarmoniCa**. It is composed of the following two techniques to alleviate the discrepancies mentioned above. Detailed algorithms of HarmoniCa can be found in Sec. A.

Step-wise denoising training. To mitigate the first discrepancy, as shown in Fig. 4 (a), we propose a new training paradigm named *Step-Wise Denoising Training* (SDT), which completes the entire denoising process over T timesteps, thereby accounting for the cache usage and update from all prior timesteps. Specifically, at timestep T , we randomly sample a Gaussian noise x_T and perform a single denoising step to pre-fill the cache. Over the following $T - 1$ timesteps, The student model, which employs the feature cache mechanism, gradually removes noise to generate an image.

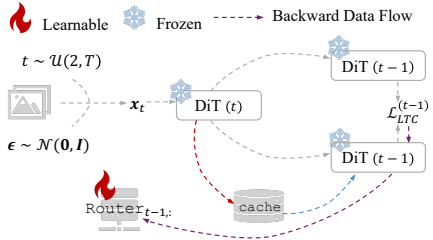


Figure 3: Training paradigm of Learning-to-Cache. $\mathcal{L}_{LTC}^{(t)}$ denotes the loss function. In each iteration, this method manually adds noise to images to obtain x_t as the input of DiT at t . “*” in “DiT (*)” represents the current timestep.

⁴ $r_{t,i}$ in the Router is a learnable parameter.

Concurrently, the teacher model executes the same task without utilizing the `cache`. Requiring the student to mimic the output representation of its teacher, we compute the loss function and perform back-propagation to update $\text{Router}_{t,i}$ at each timestep t . To ensure that each $r_{t,i}$ is differentiable during training, distinct from Eq. (3), we proportionally combine the directly computed feature with the cached one to obtain o_i following Ma et al. (2024b):

$$o_i = r_{t,i}b_i(\mathbf{h}_i, \mathbf{cs}) + (1 - r_{t,i})c_i. \quad (5)$$

Similar to inference, we also update c_i in the `cache` with $b_i(\mathbf{h}_i, \mathbf{cs})$ when $r_{t,i} > \tau$. To improve training stability (Wimbauer et al., 2024), we fetch the output from the student as the input to the teacher for the next iteration. We repeat the above T learning iterations until the end of training.

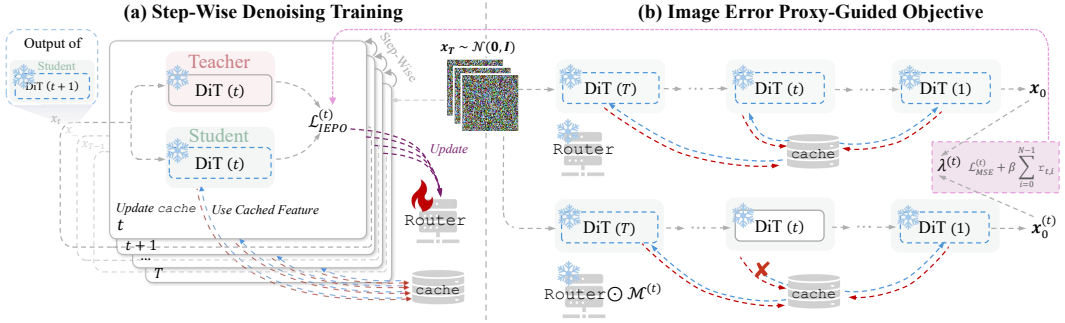


Figure 4: Overview of HarmoniCa. (a) *Step-Wise Denoising Training* (SDT) mimics the multi-timestep inference stage, which integrates the impact of prior timesteps at t . (b) *Image-Error Proxy-Guided Objective* (IEPO) incorporates the final image error into the learning objective by an efficient proxy $\lambda^{(t)}$, which is updated through gradient-free image generation passes every C training iterations. $\mathcal{M}^{(t)}$ masks the Router to disable the impact of the cache mechanism at t . \odot denotes the operation of element-wise multiplication.

As depicted in Fig. 5, by incorporating prior denoising timesteps during training, SDT significantly reduces error at each timestep and obtains a much more accurate image x_0 , even with lower computation, compared to Learning-to-Cache.

Image error proxy-guided objective. For the second discrepancy, a straightforward solution to align the target with inference involves using the error of final image x_0 caused by `cache` usage directly with a regularization term of Router as our training objective. However, even for DiT-XL/2 256×256 (Peebles & Xie, 2023) with a small training batch size, this requires approximately $5 \times$ GPU memory and $10 \times$ time compared to SDT combined with $\mathcal{L}_{LTC}^{(t)}$ as detailed in Sec. B, making it impractical. Therefore, we have to identify a proxy for the error of x_0 that can be integrated into the learning objective.

Based on the above analysis, we propose an *Image Error Proxy-guided Objective* (IEPO). It is defined at each timestep t as follows:

$$\mathcal{L}_{IEPO}^{(t)} = \lambda^{(t)} \mathcal{L}_{MSE}^{(t)} + \beta \sum_{i=0}^{N-1} r_{t,i}, \quad (6)$$

where $\lambda^{(t)}$ is our final image error proxy treated as a coefficient of $\mathcal{L}_{MSE}^{(t)}$. This proxy represents the final image error caused by the `cache` usage at t . With a large $\lambda^{(t)}$, $\mathcal{L}_{MSE}^{(t)}$ prioritizes reduction of the output error at t . This tends to decrease the cached feature usage rate at the corresponding timestep, and vice versa. Therefore, our proposed objective considers the trade-off between the error of x_0 and the `cache` usage at a certain denoising step.

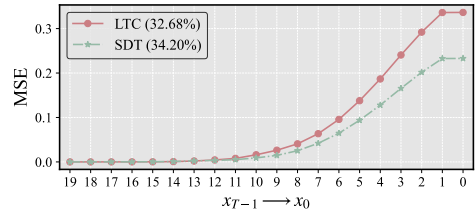


Figure 5: MSE of x_t for DiT-XL/2 256×256 (Peebles & Xie, 2023) ($T = 20, N = 56$) induced by different feature cache methods. x_t is the noisy image obtained at timestep $t + 1$. “LTC” denotes Learning-to-Cache. For a fair comparison, $\mathcal{L}_{LTC}^{(t)}$ is employed for SDT. We mark the CUR in the brackets.

Here, we detail the process to obtain $\lambda^{(t)}$ as follows. For a given Router, a mask matrix is defined to disable the use of cached features and force updating the entire cache at t as:

$$\mathcal{M}_{j,k}^{(t)} = \begin{cases} 1, & j \neq t \\ \frac{1}{r_{j,k}}, & j = t \end{cases} \quad (7)$$

where (j, k) ⁵ denotes the index of $\mathcal{M}^{(t)} \in \mathbb{R}^{T \times N}$. As depicted in Fig. 4 (b), \mathbf{x}_0 and $\mathbf{x}_0^{(t)}$ are final images generated from a randomly sampled Gaussian noise \mathbf{x}_T using feature cache guided by (Upper) Router and (Lower) Router element-wise multiplied by $\mathcal{M}^{(t)}$, respectively. Then, we can formulate $\lambda^{(t)}$ as:

$$\lambda^{(t)} = \|\mathbf{x}_0 - \mathbf{x}_0^{(t)}\|_F^2, \quad (8)$$

where $\|\cdot\|_F$ denotes the Frobenius norm. To adapt to the training dynamics, we periodically update all the coefficients $\{\lambda^{(1)}, \dots, \lambda^{(T)}\}$ every \mathbb{C} iterations⁶, instead of employing static ones.

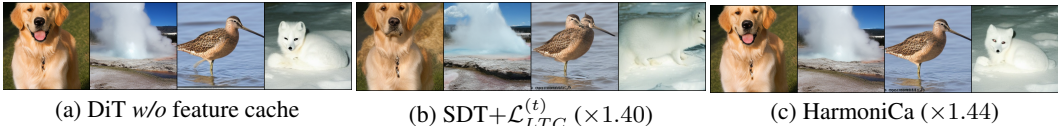


Figure 6: Random samples for DiT-XL/2 256×256 (Peebles & Xie, 2023) w/ and w/o feature cache ($T = 20$). We mark the speedup ratio in the brackets.

Fig. 6 shows that $\mathcal{L}_{IEPO}^{(t)}$ helps yield much more accurate objective-level traits and significantly improves the quality of \mathbf{x}_0 even at a higher speedup ratio than $\mathcal{L}_{LTC}^{(t)}$. The study in Sec. C justifies that employing $\mathcal{L}_{LTC}^{(t)}$ incurs the optimization deviating from minimizing the error of \mathbf{x}_0 .

4.3 EFFICIENCY DISCUSSION

Training efficiency. Our HarmoniCa incurs significantly lower training costs than the previous learning-based method. As shown in Tab. 1, HarmoniCa requires no training images, whereas Learning-to-Cache utilizes original training datasets. Thus, it is challenging to apply Learning-to-Cache to models like the PIXART- α (Chen et al., 2023) family, which are trained on large datasets, limiting its applicability. Moreover, while dynamic update of $\lambda^{(t)}$ incurs approximately 10% extra time overhead, HarmoniCa requires only three-quarters of the training hours compared to Learning-to-Cache, which needs to pre-fill the cache for each training iteration.

Inference efficiency. Fortunately, our method with a pre-learned Router has no computational overhead during runtime. Moreover, less than 6% extra memory overhead⁷ is induced by cache for DiT-XL/2 256×256 with a batch size of 8. Therefore, the introduced inference cost is controlled at a small level.

Table 1: Training costs of learning-based feature cache methods for DiT-XL/2 256×256 (Peebles & Xie, 2023) ($T = 20$). We train with all methods for 20K iterations using a global batch size 64 on 4 NVIDIA H800 80GB GPUs. For HarmoniCa, we set $\mathbb{C} = 500$. As in the original paper, we utilize the full ImageNet training set (Russakovsky et al., 2015) for Learning-to-Cache.

Method	#Images	Time(h)	Memory(GB/GPU)
Learning-to-Cache	1.22M	2.15	33.33
SDT+ $\mathcal{L}_{LTC}^{(t)}$	0	1.47	33.28
HarmoniCa	0	1.63	33.28

5 EXPERIMENTS

This section begins by outlining the detailed experimental protocols (Sec. 5.1). Subsequently, we provide comprehensive comparisons across different methods to show the superior performance and acceleration ratio of our HarmoniCa (Sec. 5.2). Finally, we provide ablation studies for the key designs of our method (Sec. 5.3).

⁵ $1 \leq j \leq T$ and $0 \leq k \leq N - 1$.

⁶ $\mathbb{C} \bmod T = 0$.

⁷The cache occupies 0.49 GB GPU memory and inference without the feature cache mechanism takes 8.18 GB GPU memory.

5.1 IMPLEMENTATION DETAILS

Models and datasets. We conduct experiments on two different image generation tasks. For class-conditional task, we employ DiT-XL/2 (Peebles & Xie, 2023) 256×256 and 512×512 models pre-trained and accessed on ImageNet dataset (Russakovsky et al., 2015). For text-to-image (T2I) task, we utilize PIXART- α (Chen et al., 2023) series, known for its outstanding performance. These models including PIXART-XL/2 at resolutions of 256×256 and 512×512 , along with PIXART-XL/2-1024-MS at a higher resolution of 1024×1024 , are tested on MS-COCO dataset (Lin et al., 2015). We additionally use T5 model (Raffel et al., 2023) as their text encoders.

Training settings. Following Ma et al. (2024b), we set the threshold τ as 0.1 for all the models. Each of them is trained for 20K iterations employing the AdamW optimizer (Loshchilov & Hutter, 2019) on 4 NVIDIA H800 80GB GPUs. The learning rate is fixed at 0.01, C is set to 500, and global batch sizes of 64, 48, and 32 are utilized for models with increasing resolutions. Additionally, we collect 1000 MS-COCO captions for T2I training.

Baselines. For class-conditional experiments, we choose the current state-of-the-art (SOTA) Learning-to-Cache (Ma et al., 2024b) as our baseline. Due to the limits mentioned in Sec. 4.3, we employ FORA (Selvaraju et al., 2024) and Δ -DiT (Chen et al., 2024b), excluding Learning-to-Cache for the T2I task. The results of these methods are obtained either by re-running their open-source code (if available) or by using the data provided in the original papers, all under the same conditions as our experiments. We also report the performance of models with reduced denoising steps.

Evaluation. To assess the generation quality, Fréchet Inception Distance (FID) (Nash et al., 2021), and sFID (Nash et al., 2021) are applied to all experiments. For DiT-XL-2, we additionally provide Inception Score (IS) (Salimans et al., 2016), Precision, and Recall (Kynkäänniemi et al., 2019) as reference metrics. For PIXART- α , to gauge the compatibility of image-caption pairs, we calculate CLIP score (Hessel et al., 2022) using ViT-B/32 (Dosovitskiy et al., 2020) as the backbone. To evaluate the inference efficiency, we measure the CUR⁸ and the inference latency for a batch size of 8. In detail, we sample 50K images adopting DDIM (Song et al., 2020a) for DiT-XL/2, and 30K images utilizing IDDPM (Nichol & Dhariwal, 2021), DPM-Solver++ (Lu et al., 2022b), and SA-Solver (Xue et al., 2024) for PIXART- α . All of them use classifier-free guidance (cf_g) (Ho & Salimans, 2022).

More implementation details can be found in Sec. D and the results of PIXART- Σ (Chen et al., 2024a) family are available in Sec. E, including generation with an extremely high-resolution of 2048×2048 . In addition, we also present the results of combination with quantization to further accelerate DiT inference in Sec. F.

5.2 MAIN RESULTS

Class-conditional generation. We begin our evaluation with DiT-XL/2 on ImageNet and compare it with current SOTA Learning-to-Cache (Ma et al., 2024b) and the approach employing fewer timesteps. The results are presented in Tab. 2, where our HarmoniCa surpasses baseline methods. Notably, with a higher speedup ratio for a 10-step DiT-XL/2 256×256 , HarmoniCa achieves an FID of 13.35 and an IS of 206.57, outperforming Learning-to-Cache by 1.24 and 5.20, respectively. Moreover, the superiority of our HarmoniCa increases as the number of timesteps decreases. We conjecture that it is because the difficulty to learn a Router rises as the timestep goes up. Additionally, we further conduct experiments with a lower CUR for this task in Sec. H.

T2I generation. We also present PixArt- α results in Tab. 3, comparing our HarmoniCa against FORA (Selvaraju et al., 2024) and the method using fewer timesteps. HarmoniCa outperforms these benchmarks across all metrics. For example, with the 20-step DPM-Solver++, PIXART- α 256×256 employing HarmoniCa achieves an FID of 27.61 and speeds up by $1.52\times$, surpassing the non-accelerated model’s FID of 27.68. In contrast, DPM-Solver++ with 15 steps and FORA only achieves FIDs of 31.68 and 38.20, respectively, with speed increases under $1.32\times$. Notably, HarmoniCa also cuts about 36% off processing time without dropping performance when using the IDDPM sampler, while FORA results in over a 20 FID increase and a 15.67% CUR decrease. Overall, our method consistently delivers superior performance and speedup improvements across

⁸Definition can be found in Sec. 3.

Table 2: Accelerating image generation on ImageNet for the DiT-XL/2. We mark the speedup ratio in the brackets and highlight the **best score** in bold.

Method	T	IS \uparrow	FID \downarrow	sFID \downarrow	Prec. \uparrow	Recall \uparrow	CUR(%) \uparrow	Latency(s) \downarrow
DiT-XL/2 256 \times 256 (c $\bar{f}g = 1.5$)								
DDIM (Song et al., 2020a)	50	240.37	2.27	4.25	80.25	59.77	-	1.767
DDIM (Song et al., 2020a)	39	237.84	2.37	4.32	80.22	59.31	-	1.379 _($\times 1.28$)
Learning-to-Cache (Ma et al., 2024b)	50	233.26	2.62	4.50	79.40	59.15	23.39	1.419 _($\times 1.25$)
HarmoniCa	50	238.74	2.36	4.24	80.57	59.68	23.68	1.361 _($\times 1.30$)
DDIM (Song et al., 2020a)	20	224.37	3.52	4.96	78.47	58.33	-	0.658
DDIM (Song et al., 2020a)	14	201.83	5.77	6.61	75.14	55.08	-	0.466 _($\times 1.41$)
Learning-to-Cache (Ma et al., 2024b)	20	201.37	5.34	6.36	75.04	56.09	35.60	0.468 _($\times 1.41$)
HarmoniCa	20	206.57	4.88	5.91	75.20	58.74	37.50	0.456 _($\times 1.44$)
DDIM (Song et al., 2020a)	10	159.93	12.16	11.31	67.10	52.27	-	0.332
DDIM (Song et al., 2020a)	9	140.37	16.54	14.44	62.63	50.08	-	0.299 _($\times 1.11$)
Learning-to-Cache (Ma et al., 2024b)	10	145.09	14.59	11.58	64.03	52.06	19.11	0.279 _($\times 1.19$)
HarmoniCa	10	151.83	13.35	11.13	65.22	52.18	22.86	0.270 _($\times 1.23$)
DiT-XL/2 512 \times 512 (c $\bar{f}g = 1.5$)								
DDIM (Song et al., 2020a)	20	184.47	5.10	5.79	81.77	54.50	-	3.356
DDIM (Song et al., 2020a)	16	173.31	6.47	6.67	81.10	51.30	-	2.688 _($\times 1.25$)
Learning-to-Cache (Ma et al., 2024b)	20	178.11	6.24	7.01	81.21	53.30	23.57	2.633 _($\times 1.28$)
HarmoniCa	20	179.84	5.72	6.61	81.33	55.80	25.98	2.574 _($\times 1.30$)

different resolutions and samplers, demonstrating its efficacy. HarmoniCa also significantly outperforms Δ -DiT (Chen et al., 2024b), which can be found in Sec. I.

Table 3: Accelerating image generation on MS-COCO for the PIXART- α .

Method	T	CLIP \uparrow	FID \downarrow	sFID \downarrow	CUR(%) \uparrow	Latency(s) \downarrow
PIXART- α 256 \times 256 (c $\bar{f}g = 4.5$)						
DPM-Solver++ (Lu et al., 2022b)	20	30.96	27.68	36.39	-	0.553
DPM-Solver++ (Lu et al., 2022b)	15	30.77	31.68	38.92	-	0.418 _($\times 1.32$)
FORA (Selvaraju et al., 2024)	20	-	38.20	-	50.00	0.424 _($\times 1.30$)
HarmoniCa	20	30.93	27.61	37.48	65.02	0.364 _($\times 1.52$)
IDDPM (Nichol & Dhariwal, 2021)	100	31.25	24.15	33.65	-	2.572
IDDPM (Nichol & Dhariwal, 2021)	75	31.25	24.17	33.73	-	1.868 _($\times 1.37$)
FORA (Selvaraju et al., 2024)	100	-	55.30	-	50.00	1.889 _($\times 1.36$)
HarmoniCa	100	31.23	23.79	32.49	65.67	1.641 _($\times 1.56$)
SA-Solver (Xue et al., 2024)	25	31.31	23.76	34.93	-	0.891
SA-Solver (Xue et al., 2024)	20	31.28	23.96	35.63	-	0.677 _($\times 1.31$)
HarmoniCa	25	31.29	23.85	35.56	54.31	0.665 _($\times 1.34$)
PIXART- α 512 \times 512 (c $\bar{f}g = 4.5$)						
DPM-Solver++ (Lu et al., 2022b)	20	31.30	23.96	40.34	-	1.759
DPM-Solver++ (Lu et al., 2022b)	15	31.29	25.12	40.37	-	1.291 _($\times 1.36$)
HarmoniCa	20	31.30	24.99	40.36	55.01	1.168 _($\times 1.51$)
PIXART- α 1024 \times 1024 (c $\bar{f}g = 4.5$)						
DPM-Solver++ (Lu et al., 2022b)	20	31.10	25.01	37.80	-	9.470
DPM-Solver++ (Lu et al., 2022b)	15	31.07	25.77	42.50	-	7.141 _($\times 1.32$)
HarmoniCa	20	31.08	24.76	41.83	59.65	6.289 _($\times 1.51$)

5.3 ABLATION STUDIES

In this subsection, we employ a 20-step DDIM (Song et al., 2020a) sampler for DiT-XL/2 256 \times 256 and settings in Sec. 5.1 without special claim.

Effect of different components. To show the effectiveness of components involved in HarmoniCa, we apply different combinations of training techniques and show the results in Tab. 4. For the training paradigm, equipped with $\mathcal{L}_{LTC}^{(t)}$, our SDT significantly decreases FID by 10 compared to that of Learning-to-Cache. For the learning objective, our IEPO achieves nearly a 40 IS improvement and a

Table 4: Ablation results of different components. The first row denotes the model *w/o* feature cache. The second and last rows denote **Learning-to-Cache** and **HarmoniCa**, respectively.

Training Paradigm		Learning Objective		IS \uparrow	FID \downarrow	sFID \downarrow	CUR(%) \uparrow	Latency(s) \downarrow
Learning-to-Cache	SDT	$\mathcal{L}_{LTC}^{(t)}$	$\mathcal{L}_{IEPO}^{(t)}$					
				224.37	3.52	4.96	-	0.658
✓		✓		115.00	18.57	16.18	32.68	0.483($\times 1.36$)
✓			✓	203.41	5.20	6.07	36.70	0.458($\times 1.44$)
	✓	✓		166.65	8.01	7.62	34.20	0.471($\times 1.40$)
	✓		✓	206.67	4.88	5.91	37.50	0.456 ($\times 1.44$)

3.13 FID reduction for SDT compared with $\mathcal{L}_{LTC}^{(t)}$. Moreover, both SDT and IEPO can help significantly enhance performance for the counterparts in the table. For a fair comparison, we modify the implementation of Learning-to-Cache to train the entire Router in Tab. 4. A detailed discussion of this can be found in Sec. J.

Effect of iteration interval C. As illustrated in Fig. 7, we carry out experiments to evaluate the impact of varying C values on updating $\lambda^{(t)}$ in Eq. (8). Despite similar speedup ratios, using an extreme C value leads to notable performance degradation. Specifically, a large C means the proxy $\lambda^{(t)}$ fails to accurately and timely reflect the cache mechanism’s effect on the final image. Conversely, a small C results in overly frequent updates, complicating training convergence. Hence, we choose a moderate value of 500 as C in this paper based on its superior performance, as demonstrated in the figure.

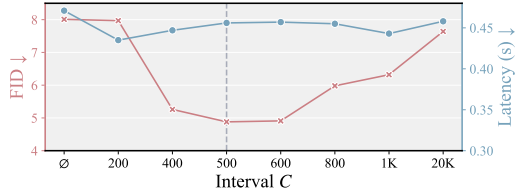


Figure 7: Ablation results of iteration interval C. \emptyset denotes the model employing $\mathcal{L}_{LTC}^{(t)}$ as its loss function.

Effect of coefficient β . We also explore the trade-off between inference speed and performance for different values of β in Eq. (6). As shown in Fig. 8, a higher β leads to greater acceleration but at the cost of more pronounced performance degradation, and vice versa. Notably, performance declines gradually when $\beta \leq 8e^{-8}$ and more sharply outside this range. This observation suggests the potential for autonomously finding an optimal β to balance speed and performance, which we aim to address in future research.

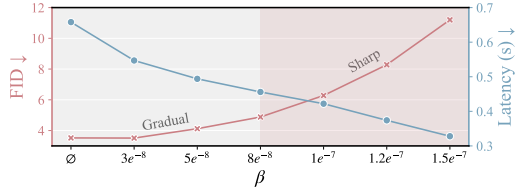


Figure 8: Ablation results of coefficient β in Eq. (6). \emptyset denotes the model *w/o* feature cache.

Effect of different metrics for $\lambda^{(t)}$. In Tab. 5, we conduct experiments to explore the effect of $\lambda^{(t)}$ with different metrics. Both $\|\cdot\|_F^2$ and $\mathcal{D}_{KL}(\cdot)$ lead to notable performance enhancements compared to using only the output error (*i.e.*, $\lambda^{(t)} = 1$) at each time step. Due to the insensitivity to outliers, $\sum|\cdot|$ is generally less effective for image reconstruction and inferior to the others in Tab. 5.

Table 5: Ablation results of different metrics for $\lambda^{(t)}$. The first and second columns represent the model *w/o* feature cache and SDD+ $\mathcal{L}_{LTC}^{(t)}$, respectively. $\mathcal{D}_{KL}(\cdot)$ denotes Kullback–Leibler (KL) divergence.

$\lambda^{(t)}$	$+\infty$	1	$\sum x_0 - x_0^{(t)} $	$\ x_0 - x_0^{(t)}\ _F^2$	$\mathcal{D}_{KL}(x_0, x_0^{(t)})$
IS \uparrow	224.37	166.65	172.08	206.57	205.91
FID \downarrow	3.52	8.01	6.95	4.88	5.25
sFID \downarrow	4.96	7.62	7.79	5.91	5.51
CUR(%) \uparrow	-	34.20	34.82	37.50	36.79
Latency(s) \downarrow	0.658	0.471($\times 1.40$)	0.470($\times 1.40$)	0.456 ($\times 1.44$)	0.458($\times 1.44$)

6 CONCLUSION

In this research, we focus on accelerating Diffusion Transformers (DiTs) through the cache mechanism in a learning-based way. We first identify two discrepancies between training and inference of the previous method: (1) *Prior Timestep Disregard* in which earlier step influences are neglected, leading to inconsistency with inference, and (2) *Objective Mismatch*, where training focuses on

intermediate results, misaligning with the final image quality target. To alleviate these discrepancies, we **Harmonize** training and inference by introducing a novel feature Cache framework dubbed **HarmoniCa**, which consists of the *Step-wise Denoising Training* (SDT) and the *Image Error-Aware Optimization Objective* (IEPO). SDT captures the influence of all timesteps during training, closing the gap with the inference stage, while IEPO introduces an efficient proxy for final image error, ensuring that optimization objectives remain aligned with inference requirements. With the combination of the two components, extensive experiments demonstrate that our framework achieves superior performance and efficiency with significantly lower training costs compared to the existing training-based method.

ACKNOWLEDGEMENT

We thank Chengtao Lv and Yuyang Chen for their insights and feedback, and Yifu Ding for her help with the paper’s diagrams.

REFERENCES

- Kushal Arora, Layla El Asri, Hareesh Bahuleyan, and Jackie Cheung. Why exposure bias matters: An imitation learning perspective of error accumulation in language generation. In Smaranda Muresan, Preslav Nakov, and Aline Villavicencio (eds.), *Findings of the Association for Computational Linguistics: ACL 2022*, pp. 700–710, Dublin, Ireland, May 2022. Association for Computational Linguistics. doi: 10.18653/v1/2022.findings-acl.58. URL <https://aclanthology.org/2022.findings-acl.58>.
- Andreas Blattmann, Tim Dockhorn, Sumith Kulal, Daniel Mendelevitch, Maciej Kilian, Dominik Lorenz, Yam Levi, Zion English, Vikram Voleti, Adam Letts, et al. Stable video diffusion: Scaling latent video diffusion models to large datasets. *arXiv preprint arXiv:2311.15127*, 2023.
- Junsong Chen, Jincheng Yu, Chongjian Ge, Lewei Yao, Enze Xie, Yue Wu, Zhongdao Wang, James Kwok, Ping Luo, Huchuan Lu, et al. Pixart- α : Fast training of diffusion transformer for photorealistic text-to-image synthesis. *arXiv preprint arXiv:2310.00426*, 2023.
- Junsong Chen, Chongjian Ge, Enze Xie, Yue Wu, Lewei Yao, Xiaozhe Ren, Zhongdao Wang, Ping Luo, Huchuan Lu, and Zhenguo Li. Pixart- σ : Weak-to-strong training of diffusion transformer for 4k text-to-image generation. *arXiv preprint arXiv:2403.04692*, 2024a.
- Pengtao Chen, Mingzhu Shen, Peng Ye, Jianjian Cao, Chongjun Tu, Christos-Savvas Bouganis, Yiren Zhao, and Tao Chen. δ -dit: A training-free acceleration method tailored for diffusion transformers, 2024b. URL <https://arxiv.org/abs/2406.01125>.
- Prafulla Dhariwal and Alexander Nichol. Diffusion models beat gans on image synthesis. *Advances in neural information processing systems*, 34:8780–8794, 2021.
- Alexey Dosovitskiy, Lucas Beyer, Alexander Kolesnikov, Dirk Weissenborn, Xiaohua Zhai, Thomas Unterthiner, Mostafa Dehghani, Matthias Minderer, Georg Heigold, Sylvain Gelly, et al. An image is worth 16x16 words: Transformers for image recognition at scale. *arXiv preprint arXiv:2010.11929*, 2020.
- Patrick Esser, Sumith Kulal, Andreas Blattmann, Rahim Entezari, Jonas Müller, Harry Saini, Yam Levi, Dominik Lorenz, Axel Sauer, Frederic Boesel, et al. Scaling rectified flow transformers for high-resolution image synthesis. In *Forty-first International Conference on Machine Learning*, 2024.
- Gongfan Fang, Xinyin Ma, and Xinchao Wang. Structural pruning for diffusion models, 2023. URL <https://arxiv.org/abs/2305.10924>.
- Kaiming He, Xiangyu Zhang, Shaoqing Ren, and Jian Sun. Deep residual learning for image recognition. In *Proceedings of the IEEE conference on computer vision and pattern recognition*, pp. 770–778, 2016.

- Yefei He, Jing Liu, Weijia Wu, Hong Zhou, and Bohan Zhuang. Efficientdm: Efficient quantization-aware fine-tuning of low-bit diffusion models, 2024. URL <https://arxiv.org/abs/2310.03270>.
- Jack Hessel, Ari Holtzman, Maxwell Forbes, Ronan Le Bras, and Yejin Choi. Clipscore: A reference-free evaluation metric for image captioning, 2022.
- Martin Heusel, Hubert Ramsauer, Thomas Unterthiner, Bernhard Nessler, and Sepp Hochreiter. Gans trained by a two time-scale update rule converge to a local nash equilibrium, 2018. URL <https://arxiv.org/abs/1706.08500>.
- Jonathan Ho and Tim Salimans. Classifier-free diffusion guidance. *arXiv preprint arXiv:2207.12598*, 2022.
- Jonathan Ho, Ajay Jain, and Pieter Abbeel. Denoising diffusion probabilistic models. *Advances in neural information processing systems*, 33:6840–6851, 2020.
- Jonathan Ho, Tim Salimans, Alexey Gritsenko, William Chan, Mohammad Norouzi, and David J. Fleet. Video diffusion models, 2022. URL <https://arxiv.org/abs/2204.03458>.
- Edward J. Hu, Yelong Shen, Phillip Wallis, Zeyuan Allen-Zhu, Yuanzhi Li, Shean Wang, Lu Wang, and Weizhu Chen. Lora: Low-rank adaptation of large language models, 2021. URL <https://arxiv.org/abs/2106.09685>.
- Yushi Huang, Ruihao Gong, Jing Liu, Tianlong Chen, and Xianglong Liu. Tfmq-dm: Temporal feature maintenance quantization for diffusion models. In *Proceedings of the IEEE/CVF Conference on Computer Vision and Pattern Recognition*, pp. 7362–7371, 2024.
- Alexia Jolicœur-Martineau, Ke Li, Rémi Piché-Taillefer, Tal Kachman, and Ioannis Mitliagkas. Gotta go fast when generating data with score-based models. *arXiv preprint arXiv:2105.14080*, 2021.
- Andrew Kerr, Duane Merrill, Julien Demouth, and John Tran. Cutlass: Fast linear algebra in cuda c++. *NVIDIA Developer Blog*, 2017.
- Zhifeng Kong and Wei Ping. On fast sampling of diffusion probabilistic models. *arXiv preprint arXiv:2106.00132*, 2021.
- Tuomas Kynkäänniemi, Tero Karras, Samuli Laine, Jaakko Lehtinen, and Timo Aila. Improved precision and recall metric for assessing generative models. *Advances in neural information processing systems*, 32, 2019.
- Mingxiao Li, Tingyu Qu, Ruicong Yao, Wei Sun, and Marie-Francine Moens. Alleviating exposure bias in diffusion models through sampling with shifted time steps, 2024. URL <https://arxiv.org/abs/2305.15583>.
- Senmao Li, Taihang Hu, Fahad Shahbaz Khan, Linxuan Li, Shiqi Yang, Yaxing Wang, Ming-Ming Cheng, and Jian Yang. Faster diffusion: Rethinking the role of unet encoder in diffusion models. *arXiv preprint arXiv:2312.09608*, 2023a.
- Xiuyu Li, Yijiang Liu, Long Lian, Huanrui Yang, Zhen Dong, Daniel Kang, Shanghang Zhang, and Kurt Keutzer. Q-diffusion: Quantizing diffusion models. In *Proceedings of the IEEE/CVF International Conference on Computer Vision*, pp. 17535–17545, 2023b.
- Tsung-Yi Lin, Michael Maire, Serge Belongie, Lubomir Bourdev, Ross Girshick, James Hays, Pietro Perona, Deva Ramanan, C. Lawrence Zitnick, and Piotr Dollár. Microsoft coco: Common objects in context, 2015. URL <https://arxiv.org/abs/1405.0312>.
- Enshu Liu, Xuefei Ning, Zinan Lin, Huazhong Yang, and Yu Wang. Oms-dpm: Optimizing the model schedule for diffusion probabilistic models. In *International Conference on Machine Learning*, pp. 21915–21936. PMLR, 2023.
- Luping Liu, Yi Ren, Zhijie Lin, and Zhou Zhao. Pseudo numerical methods for diffusion models on manifolds. *arXiv preprint arXiv:2202.09778*, 2022.

- Ilya Loshchilov and Frank Hutter. Decoupled weight decay regularization, 2019. URL <https://arxiv.org/abs/1711.05101>.
- Cheng Lu, Yuhao Zhou, Fan Bao, Jianfei Chen, Chongxuan Li, and Jun Zhu. Dpm-solver: A fast ode solver for diffusion probabilistic model sampling in around 10 steps. *Advances in Neural Information Processing Systems*, 35:5775–5787, 2022a.
- Cheng Lu, Yuhao Zhou, Fan Bao, Jianfei Chen, Chongxuan Li, and Jun Zhu. Dpm-solver++: Fast solver for guided sampling of diffusion probabilistic models. *arXiv preprint arXiv:2211.01095*, 2022b.
- Eric Luhman and Troy Luhman. Knowledge distillation in iterative generative models for improved sampling speed. *arXiv preprint arXiv:2101.02388*, 2021.
- Xin Ma, Yaohui Wang, Gengyun Jia, Xinyuan Chen, Ziwei Liu, Yuan-Fang Li, Cunjian Chen, and Yu Qiao. Latte: Latent diffusion transformer for video generation. *arXiv preprint arXiv:2401.03048*, 2024a.
- Xinyin Ma, Gongfan Fang, Michael Bi Mi, and Xinchao Wang. Learning-to-cache: Accelerating diffusion transformer via layer caching, 2024b. URL <https://arxiv.org/abs/2406.01733>.
- Xinyin Ma, Gongfan Fang, and Xinchao Wang. Deepcache: Accelerating diffusion models for free. In *Proceedings of the IEEE/CVF Conference on Computer Vision and Pattern Recognition*, pp. 15762–15772, 2024c.
- Markus Nagel, Marios Fournarakis, Rana Ali Amjad, Yelysei Bondarenko, Mart van Baalen, and Tijmen Blankevoort. A white paper on neural network quantization, 2021. URL <https://arxiv.org/abs/2106.08295>.
- Charlie Nash, Jacob Menick, Sander Dieleman, and Peter W Battaglia. Generating images with sparse representations. *arXiv preprint arXiv:2103.03841*, 2021.
- Alexander Quinn Nichol and Prafulla Dhariwal. Improved denoising diffusion probabilistic models. In *International conference on machine learning*, pp. 8162–8171. PMLR, 2021.
- Mang Ning, Enver Sangineto, Angelo Porrello, Simone Calderara, and Rita Cucchiara. Input perturbation reduces exposure bias in diffusion models, 2023. URL <https://arxiv.org/abs/2301.11706>.
- Mang Ning, Mingxiao Li, Jianlin Su, Albert Ali Salah, and Itir Onal Ertugrul. Elucidating the exposure bias in diffusion models, 2024. URL <https://arxiv.org/abs/2308.15321>.
- Zizheng Pan, Bohan Zhuang, De-An Huang, Weili Nie, Zhiding Yu, Chaowei Xiao, Jianfei Cai, and Anima Anandkumar. T-stitch: Accelerating sampling in pre-trained diffusion models with trajectory stitching. *arXiv preprint arXiv:2402.14167*, 2024.
- William Peebles and Saining Xie. Scalable diffusion models with transformers. In *Proceedings of the IEEE/CVF International Conference on Computer Vision*, pp. 4195–4205, 2023.
- Dustin Podell, Zion English, Kyle Lacey, Andreas Blattmann, Tim Dockhorn, Jonas Müller, Joe Penna, and Robin Rombach. Sdxl: Improving latent diffusion models for high-resolution image synthesis, 2023. URL <https://arxiv.org/abs/2307.01952>.
- Colin Raffel, Noam Shazeer, Adam Roberts, Katherine Lee, Sharan Narang, Michael Matena, Yanqi Zhou, Wei Li, and Peter J. Liu. Exploring the limits of transfer learning with a unified text-to-text transformer, 2023. URL <https://arxiv.org/abs/1910.10683>.
- Robin Rombach, Andreas Blattmann, Dominik Lorenz, Patrick Esser, and Björn Ommer. High-resolution image synthesis with latent diffusion models. In *CVPR*, 2022.
- Olaf Ronneberger, Philipp Fischer, and Thomas Brox. U-net: Convolutional networks for biomedical image segmentation, 2015.

- Olga Russakovsky, Jia Deng, Hao Su, Jonathan Krause, Sanjeev Satheesh, Sean Ma, Zhiheng Huang, Andrej Karpathy, Aditya Khosla, Michael Bernstein, et al. Imagenet large scale visual recognition challenge. *International journal of computer vision*, 115:211–252, 2015.
- Chitwan Saharia, William Chan, Saurabh Saxena, Lala Li, Jay Whang, Emily L Denton, Kamyar Ghasemipour, Raphael Gontijo Lopes, Burcu Karagol Ayan, Tim Salimans, et al. Photorealistic text-to-image diffusion models with deep language understanding. *Advances in neural information processing systems*, 35:36479–36494, 2022.
- Tim Salimans and Jonathan Ho. Progressive distillation for fast sampling of diffusion models. *arXiv preprint arXiv:2202.00512*, 2022.
- Tim Salimans, Ian Goodfellow, Wojciech Zaremba, Vicki Cheung, Alec Radford, and Xi Chen. Improved techniques for training gans. *Advances in neural information processing systems*, 29, 2016.
- Florian Schmidt. Generalization in generation: A closer look at exposure bias. In Alexandra Birch, Andrew Finch, Hiroaki Hayashi, Ioannis Konstas, Thang Luong, Graham Neubig, Yusuke Oda, and Katsuhito Sudoh (eds.), *Proceedings of the 3rd Workshop on Neural Generation and Translation*, pp. 157–167, Hong Kong, November 2019. Association for Computational Linguistics. doi: 10.18653/v1/D19-5616. URL <https://aclanthology.org/D19-5616>.
- Pratheba Selvaraju, Tianyu Ding, Tianyi Chen, Ilya Zharkov, and Luming Liang. Fora: Fast-forward caching in diffusion transformer acceleration. *arXiv preprint arXiv:2407.01425*, 2024.
- Yuzhang Shang, Zhihang Yuan, Bin Xie, Bingzhe Wu, and Yan Yan. Post-training quantization on diffusion models. In *Proceedings of the IEEE/CVF conference on computer vision and pattern recognition*, pp. 1972–1981, 2023.
- Jiaming Song, Chenlin Meng, and Stefano Ermon. Denoising diffusion implicit models. *arXiv preprint arXiv:2010.02502*, 2020a.
- Yang Song, Jascha Sohl-Dickstein, Diederik P Kingma, Abhishek Kumar, Stefano Ermon, and Ben Poole. Score-based generative modeling through stochastic differential equations. *arXiv preprint arXiv:2011.13456*, 2020b.
- A Vaswani. Attention is all you need. *Advances in Neural Information Processing Systems*, 2017.
- Hongyu Wang, Shuming Ma, Li Dong, Shaohan Huang, Dongdong Zhang, and Furu Wei. Deepnet: Scaling transformers to 1,000 layers. *IEEE Transactions on Pattern Analysis and Machine Intelligence*, 2024a.
- Kafeng Wang, Jianfei Chen, He Li, Zhenpeng Mi, and Jun Zhu. Sparsedm: Toward sparse efficient diffusion models. *arXiv preprint arXiv:2404.10445*, 2024b.
- Felix Wimbauer, Bichen Wu, Edgar Schoenfeld, Xiaoliang Dai, Ji Hou, Zijian He, Artsiom Sanakoyeu, Peizhao Zhang, Sam Tsai, Jonas Kohler, et al. Cache me if you can: Accelerating diffusion models through block caching. In *Proceedings of the IEEE/CVF Conference on Computer Vision and Pattern Recognition*, pp. 6211–6220, 2024.
- Shuchen Xue, Mingyang Yi, Weijian Luo, Shifeng Zhang, Jiacheng Sun, Zhenguo Li, and Zhi-Ming Ma. Sa-solver: Stochastic adams solver for fast sampling of diffusion models. *Advances in Neural Information Processing Systems*, 36, 2024.
- Zhihang Yuan, Pu Lu, Hanling Zhang, Xuefei Ning, Linfeng Zhang, Tianchen Zhao, Shengen Yan, Guohao Dai, and Yu Wang. Dtfastattn: Attention compression for diffusion transformer models. *arXiv preprint arXiv:2406.08552*, 2024.
- Dingkun Zhang, Sijia Li, Chen Chen, Qingsong Xie, and Haonan Lu. Laptop-diff: Layer pruning and normalized distillation for compressing diffusion models. *arXiv preprint arXiv:2404.11098*, 2024.
- Qinsheng Zhang and Yongxin Chen. Fast sampling of diffusion models with exponential integrator. *arXiv preprint arXiv:2204.13902*, 2022.

Qinsheng Zhang, Molei Tao, and Yongxin Chen. gddim: Generalized denoising diffusion implicit models. *arXiv preprint arXiv:2206.05564*, 2022.

Appendix

A ALGORITHM OF HARMONICA

As described in Alg. 1, we provide a detailed algorithm of our HarmoniCa. For clarity, we omit the pre-fill stage (*i.e.*, denoising at T), where `Router $_T$` : is forced to be set to $\{1\}_{1 \times N}$. The `conds` for T2I tasks and class-conditional generation are pre-prepared text prompts and class labels, respectively.

Algorithm 1 HarmoniCa: the upper snippet describes the full procedure, and the lower side contains the subroutine for computing the proxy of the final image error.

```

func HARMONICA( $\phi, \epsilon_\theta, \text{iters}, \text{conds}, \tau, \beta, T, C$ )
Require:  $\phi(\cdot)$  — diffusion sampler
            $\epsilon_\theta(\cdot)$  — DiT model
           iters — amount of training iterations
           conds — conditional inputs
            $\tau$  — threshold
            $\beta$  — constraint coefficient
            $T$  — maximum denoising step
            $C$  — iteration interval

1: Initialize Router with a normal distribution
2: cache =  $\emptyset$  ▷ Initialize cache
3: for  $i$  in 0 to  $\frac{\text{iters}}{T} - 1$  do:
4:    $\mathbf{x}_T \sim \mathcal{N}(\mathbf{0}, \mathbf{I})$ 
5:   if  $i \% \frac{C}{T} = 0$  then
6:      $\{\lambda^{(1)}, \dots, \lambda^{(T)}\} = \text{gen\_proxy}(\phi, \epsilon_\theta, \mathbf{x}_T, \text{conds}[i], \tau, \text{Router})$ 
7:   end if
8:   for  $t$  in  $T$  to 1 do:
9:      $\epsilon^{(t)'} = \epsilon_\theta(\mathbf{x}_t, t, \text{conds}[i], \text{Router}_{t,:}, \tau, \text{cache})$  ▷ Fig. 2
10:     $\epsilon^{(t)} = \epsilon_\theta(\mathbf{x}_t, t, \text{conds}[i])$ 
11:     $\mathcal{L}_{IEPO}^{(t)} = \lambda^{(t)} \|\epsilon^{(t)'} - \epsilon^{(t)}\|_F^2 + \beta \sum_{i=0}^{N-1} r_i^{(t)}$  ▷ Eq. (6)
12:    Tune Router $_{t,:}$  by back-propagation
13:     $\mathbf{x}_{t-1} = \phi(\mathbf{x}_t, t, \epsilon^{(t)'})$ 
14:  end for
15: end for
16: return Router

func gen_proxy( $\phi, \epsilon_\theta, \mathbf{x}_T, \text{cond}, \tau, \text{Router}$ )
1: cache =  $\emptyset$  ▷ Initialize cache
2: Employ feature cache guided by Router to generate  $\mathbf{x}_0$ 
3: for  $t$  in  $T$  to 1 do:
4:   Generate  $\mathcal{M}^{(t)}$  ▷ Eq. (7)
5:   Employ feature cache guided by Router  $\odot \mathcal{M}^{(t)}$  to generate  $\mathbf{x}_0^{(t)}$ 
6:    $\lambda^{(t)} = \|\mathbf{x}_0 - \mathbf{x}_0^{(t)}\|_F^2$  ▷ Eq. (8)
7: end for
8: return  $\{\lambda^{(1)}, \lambda^{(2)}, \dots, \lambda^{(T)}\}$ 

```

B IMAGE ERROR WITH ROUTER REGULARIZATION TERM AS TRAINING OBJECTIVE

In Tab. A, $\text{SDT} + \mathcal{L}_{\mathbf{x}_0}^{(t)}$ requires $t - 1$ additional denoising passes per training iteration at t to compute the error of \mathbf{x}_0 . Consequently, this approach consumes about $\times 9.73$ GPU hours compared to $\text{SDT} + \mathcal{L}_{LTC}^{(t)}$. Due to the extensive intermediate activations stored from timestep t to 1 for back-propagation, it also costs $\times 4.90$ GPU memory. This estimation is conducted with small batch sizes and limited iterations. Therefore, $\text{SDT} + \mathcal{L}_{\mathbf{x}_0}^{(t)}$ is less feasible for models with larger latent spaces or higher token counts per image, such as DiT-XL/2 512×512 , particularly in large-batch, complete training scenarios. Additionally, the network effectively becomes $T \times N$ stacked Transformer

blocks under this strategy, making it difficult (Wang et al., 2024a) to optimize the Router with even a moderate T value, such as 50 or 100.

Table A: Training costs estimation across different methods for DiT-XL/2 256×256 (Peebles & Xie, 2023) ($T = 20$). We only employ 5K iterations with a global batch size of 8 on 4 NVIDIA H800 80G GPUs. $\mathcal{L}_{x_0}^{(t)}$ denotes the loss function replacing $\mathcal{L}_{MSE}^{(t)}$ in Eq. (4) with the final image error.

Method	#Images	Time(h)	Memory(GB/GPU)
SDM+ $\mathcal{L}_{x_0}^{(t)}$	0	1.46	65.36
SDM+ $\mathcal{L}_{LTC}^{(t)}$	0	0.15	13.33

C OPTIMIZATION DEVIATION

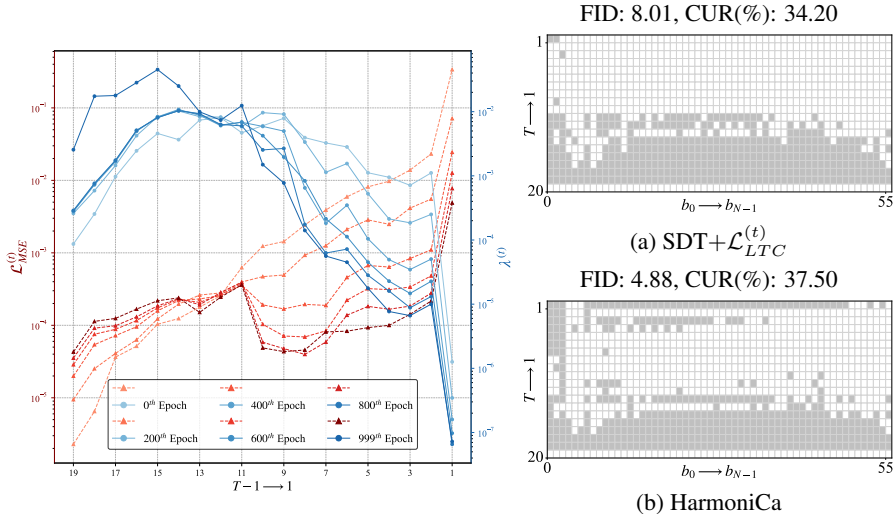


Figure A: (Left) Variations of $\mathcal{L}_{MSE}^{(t)}$ and $\lambda^{(t)}$ for SDT+ $\mathcal{L}_{LTC}^{(t)}$. (Right) Router visualization across different methods. The gray grid (t, i) represents using the feature in cache at t without computing \circ_i . The white grid indicates computing and updating cache. We also mark their FID (Heusel et al., 2018) and CUR. All the above experiments employ DiT-XL/2 256×256 ($T = 20, N = 56$).

To generate high-quality x_0 and accelerate the inference phase, we believe only considering the output error at a certain timestep can cause a deviated optimization due to its gap *w.r.t* the error of x_0 . To validate this, we plot the values of $\mathcal{L}_{MSE}^{(t)}$ in Eq. (4) and $\lambda^{(t)}$ in Eq. (8) during the training phase of SDT+ $\mathcal{L}_{LTC}^{(t)}$ in Fig. A (Left). Comparing $\mathcal{L}_{MSE}^{(t)}$ and $\lambda^{(t)}$ across different denoising steps, their results present a significant discrepancy. For instance, $\mathcal{L}_{MSE}^{(t)}$ at $t = 14$ is several orders of magnitude smaller than that at $t = 1$ during the entire training process, and the opposite situation happens for $\lambda^{(t)}$. Intuitively, this indicates that we could increase the cache usage rate at $t = 1$, and vice versa at $t = 14$ for higher performance while keeping the same speedup ratio according to the value of the proxy $\lambda^{(t)}$. However, only considering the output error at each timestep (*i.e.*, $\mathcal{L}_{MSE}^{(t)}$) can optimize towards a shifted direction. In practice, the learned Router with the guidance of $\lambda^{(t)}$ in Fig. A (Right) (b) caches less in large timesteps like $t = 14$ and reuses more in small timesteps as $t = 1$ compared to that in Fig. A (Right) (a) achieving significant performance enhancement.

D MORE IMPLEMENTATION DETAILS

In this section, we present more implementation details for our HarmoniCa. First, following Ma et al. (2024b), we also perform a sigmoid function⁹ to each $r_{t,i}$ before it is passed to the model.

⁹ $\sigma(x) = \frac{1}{1+e^{-x}}$

Moreover, unless specified otherwise, the hyper-parameter β in Eq. (6) for all experiments is given in Tab. B; any exceptions are noted in the relevant tables.

Table B: Hyper-parameter β for training the Router.

Model	DiT-XL/2				PIXART- α				PIXART- Σ	
	256 \times 256		512 \times 512		256 \times 256		512 \times 512	1024 \times 1024	1024 \times 1024	2048 \times 2048
T	10	20	50	20	20	100	25	20	20	20
β	$7e^{-8}$	$8e^{-8}$	$5e^{-8}$	$4e^{-8}$	$1e^{-3}$	$8e^{-4}$	$8e^{-4}$	$8e^{-4}$	$8e^{-4}$	$8e^{-4}$

E RESULTS FOR PIXART- Σ

In this section, we present the results for the PIXART- Σ family, including PIXART- Σ -XL/2-1024-MS and PIXART- Σ -XL/2-2K-MS. For the latter one, we test by sampling 10K images. Additionally, we train the Router with a batch size of 16 and measure latency using a batch size of 1. All other settings are consistent with those described in Sec. 5.1.

As shown in Table C, HarmoniCa achieves a $\times 1.51$ speedup along with improved CLP scores and sFID compared to the non-accelerated model for PIXART- Σ 2048 \times 2048. Notably, this is the first time for the feature cache mechanism to accelerate image generation with such a super-high resolution of 2048 \times 2048.

Table C: Accelerating image generation on MS-COCO for the PIXART- Σ .

Method	T	CLIP \uparrow	FID \downarrow	sFID \downarrow	CUR(%) \uparrow	Latency(s) \downarrow
PIXART- Σ 1024 \times 1024 (c.f.g = 4.5)						
DPM-Solver++ (Lu et al., 2022b)	20	31.37	20.98	27.47	-	9.467
DPM-Solver++ (Lu et al., 2022b)	15	31.34	21.63	28.68	-	7.100($\times 1.33$)
HarmoniCa	20	31.36	20.94	27.25	59.52	6.432 ($\times 1.47$)
PIXART- Σ 2048 \times 2048 (c.f.g = 4.5)						
DPM-Solver++ (Lu et al., 2022b)	20	31.19	23.61	51.12	-	14.198
DPM-Solver++ (Lu et al., 2022b)	15	31.26	24.40	53.34	-	9.782($\times 1.45$)
HarmoniCa	20	31.36	23.88	53.25	58.29	9.410 ($\times 1.51$)

F COMBINATION WITH QUANTIZATION

In this section, we conduct experiments to show the high compatibility of our HarmoniCa with the model quantization technique. In Tab. D, our method boosts a considerable speedup ratio from $\times 1.18$ to $\times 1.77$ with only a 0.16 FID increase for PIXART- α 256 \times 256. In the future, we will explore combining our HarmoniCa with other acceleration techniques, such as pruning and distillation, to further reduce the computational demands for DiT.

G EXPERIMENTAL DETAILS FOR QUANTIZATION

In Sec. F, we employ 8-bit channel-wise weight quantization and 8-bit layer-wise activation quantization for full-precision (FP32) DiT-XL/2 and half-precision (FP16) PIXART- α . The former uses a 20-step DDIM sampler (Song et al., 2020a), while the latter employs a DPM-Solver++ sampler (Lu et al., 2022b) with the same steps. More specifically, we use MSE initialization (Nagel et al., 2021) for quantization parameters. For the quantization-aware fine-tuning stage, we set the learning rate of LoRA (Hu et al., 2021) and activation quantization parameters to $1e^{-6}$ and that of weight quantization parameters to $1e^{-5}$, respectively. Additionally, we employ 3.2K iterations for DiT-XL/2 (Peebles & Xie, 2023) and 9.6K iterations for PIXART- α (Chen et al., 2023) on a single NVIDIA H800 80G GPU. Other settings are the same as those from the original paper (He et al., 2024). Leveraging NVIDIA CUTLASS (Kerr et al., 2017) implementation, we evaluate the latency of quantized models employing the 8-bit multiplication for all the linear layers and convolutions.

Table D: Results of the combination of our framework and an advanced quantization method: EfficientDM (He et al., 2024). IS \uparrow is for the former and CLIP \uparrow is for the latter in the table. Experimental details for quantization can be found in Sec. G. We mark the speedup ratio and the compression ratio in the brackets.

Method	IS \uparrow /CLIP \uparrow	FID \downarrow	sFID \downarrow	CUR(%) \uparrow	Latency(s) \downarrow	#Size(GB) \downarrow
DiT-XL/2 256 \times 256 (c.f.g = 1.5)						
EfficientDM (He et al., 2024)	172.70	6.10	4.55	-	0.591 _(\times1.11)	0.64 _(\times3.93)
+HarmoniCa ($\beta = 4e^{-8}$)	168.16	6.48	4.32	26.25	0.473 _(\times1.40)	0.64 _(\times3.93)
PIXART- α 256 \times 256 (c.f.g = 4.5)						
EfficientDM (He et al., 2024)	30.09	34.84	30.34	-	0.469 _(\times1.18)	0.59 _(\times1.98)
+HarmoniCa	30.23	35.00	31.38	53.34	0.301 _(\times1.77)	0.59 _(\times1.98)
PIXART- α 512 \times 512 (c.f.g = 4.5)						
EfficientDM (He et al., 2024)	30.71	25.82	41.64	-	0.461 _(\times1.20)	0.59 _(\times1.98)
+HarmoniCa	30.65	26.90	42.82	54.31	0.296 _(\times1.80)	0.59 _(\times1.98)

H COMPARISON BETWEEN LEARNING-TO-CACHE AND HARMONICa WITH A LOW CUR(%)

In this section, we compare HarmoniCa with Learning-to-Cache (Ma et al., 2024b) at a relatively low CUR(%). As shown in Tab. E, both methods achieve a similar speedup ratio and even better performance than non-accelerated models. Therefore, we employ higher CUR in Tab. 2 to show our pronounced superiority.

Table E: Comparison results between Learning-to-Cache and HarmoniCa for the DiT-XL/2 with a low CUR(%).

Method	T	IS \uparrow	FID \downarrow	sFID \downarrow	Prec. \uparrow	Recall \uparrow	CUR(%) \uparrow	Latency(s) \downarrow
DiT-XL/2 256 \times 256 (c.f.g = 1.5)								
DDIM (Song et al., 2020a)	20	224.37	3.52	4.96	78.47	58.33	-	0.658
DDIM (Song et al., 2020a)	15	214.77	4.17	5.54	77.43	56.30	-	0.564 _(\times1.17)
Learning-to-Cache (Ma et al., 2024b)	20	228.19	3.49	4.66	79.32	59.10	22.05	0.545 _(\times1.21)
HarmoniCa ($\beta = 3e^{-8}$)	20	228.79	3.51	4.76	79.43	59.32	21.07	0.547 _(\times1.20)
DiT-XL/2 512 \times 512 (c.f.g = 1.5)								
DDIM (Song et al., 2020a)	20	184.47	5.10	5.79	81.77	54.50	-	3.356
DDIM (Song et al., 2020a)	18	180.06	5.62	6.13	81.37	53.90	-	3.021 _(\times1.11)
Learning-to-Cache (Ma et al., 2024b)	20	183.57	5.45	6.05	82.10	54.90	14.64	2.927 _(\times1.15)
HarmoniCa ($\beta = 2e^{-8}$)	20	183.71	5.32	5.84	81.83	55.80	16.61	2.863 _(\times1.17)

I COMPARISON BETWEEN Δ -DiT AND HARMONICa

In this section, we compare HarmoniCa with Δ -DiT (Chen et al., 2024b). Given that the code and implementation details of Δ -DiT¹⁰ are not open source, we report results derived from the original paper. Additionally, we evaluate performance sampling 5000 images as used in that study. As depicted in Tab F, our framework further decreases 20% latency and gains 3.52 IS improvement compared with Δ -DiT for PIXART- α with a 20-step DPM-Solver++ sampler (Lu et al., 2022b).

¹⁰ Δ -DiT presents the speedup ratio based on multiply-accumulate operates (MACs). Here we report the results according to the latency in that study.

Table F: Comparison results between Δ -DiT and HarmoniCa on on MS-COCO for PIXART- α 1024 \times 1024.

Method	T	CLIP \uparrow	FID \downarrow	IS \uparrow	CUR(%) \uparrow	Speedup \uparrow
PIXART- α 1024 \times 1024 (cfg = 4.5)						
DPM-Solver++ (Lu et al., 2022b)	20	31.07	31.98	41.30	-	-
DPM-Solver++ (Lu et al., 2022b)	13	31.04	33.29	39.15	-	$\times 1.54$
Δ -DiT (Chen et al., 2024b)	20	30.40	35.88	32.22	37.49	$\times 1.49$
HarmoniCa ($\beta = 1e^{-3}$)	20	31.08	32.97	40.67	62.31	$\times 1.63$

J COMPARISON BETWEEN LEARNING-TO-CACHE WITH DIFFERENT SAMPLING STRATEGIES

For the implementation details ¹¹, Learning-to-Cache uniformly samples an even timestep t during each training iteration ¹², as opposed to sampling any timestep from the set $\{1, \dots, T\}$ as mentioned in Alg. 1 of its original paper. Consequently, according to Fig. 3, only $r_{t,i}$, where t is an odd timestep, is learnable, while the remaining values are set to one. We compare Learning-to-Cache under different sampling strategies (*i.e.*, sampling an even timestep or without this constraint for each training iteration) against HarmoniCa. As shown in Tab. G, our framework—whether training the entire Router or only parts of it (similar to the Learning-to-Cache implementation)—consistently outperforms Learning-to-Cache regardless of the sampling strategy.

It should be noted that the experiments in Sec. 5, with the exception of those in Tab. 4, use an implementation that uniformly samples an even timestep t during each training iteration. This approach achieves significantly higher performance compared to sampling without constraints.

Table G: Comparison results between Learning-to-Cache with different sampling strategies and HarmoniCa for the DiT-XL/2 256 \times 256. “♣” denotes that only parts of the Router corresponding to odd timesteps are learnable and the remaining values are set to one (*i.e.*, disable reusing cached features).

Method	T	IS \uparrow	FID \downarrow	sFID \downarrow	Prec. \uparrow	Recall \uparrow	CUR(%) \uparrow	Latency(s) \downarrow
DiT-XL/2 256 \times 256 (cfg = 1.5)								
DDIM (Song et al., 2020a)	20	224.37	3.52	4.96	78.47	58.33	-	0.658
Learning-to-Cache (Ma et al., 2024b)	20	115.00	18.57	16.18	60.35	62.98	32.68	0.483($\times 1.36$)
Learning-to-Cache♣ (Ma et al., 2024b)	20	201.37	5.34	6.36	75.04	56.09	35.60	0.468($\times 1.41$)
HarmoniCa♣ ($\beta = 3.5e^{-8}$)	20	205.39	4.86	5.92	75.06	57.97	36.07	0.463($\times 1.42$)
HarmoniCa	20	206.57	4.88	5.91	75.20	58.74	37.50	0.456 ($\times 1.44$)

K VISUALIZATION RESULTS

As demonstrated in Figures B to H, we present random samples from both the non-accelerated DiT models and ones equipped with HarmoniCa, using a fixed random seed. Our approach not only significantly accelerates inference but also produces results that closely resemble those of the original model. For a detailed comparison, zoom in to closely examine the relevant images.

¹¹Let T be an even number here.

¹²https://github.com/horseee/learning-to-cache/blob/main/DiT/train_router.py#L244-L247

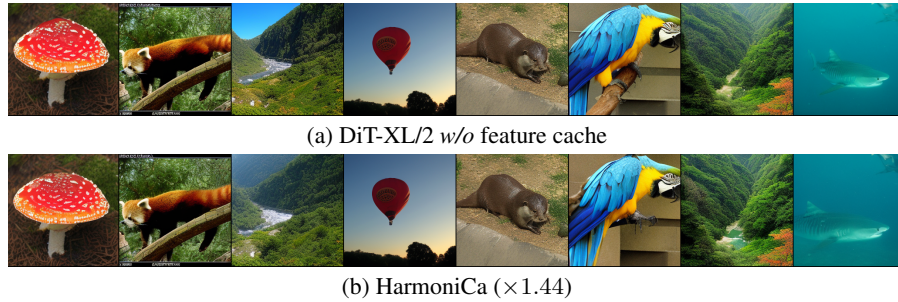


Figure B: Random samples from (a) non-accelerated and (b) accelerated DiT-XL/2 256×256 (Chen et al., 2023) with a 20-step DDIM sampler (Song et al., 2020a). The resolution of each sample is 256×256 . We mark the speedup ratio in the brackets.

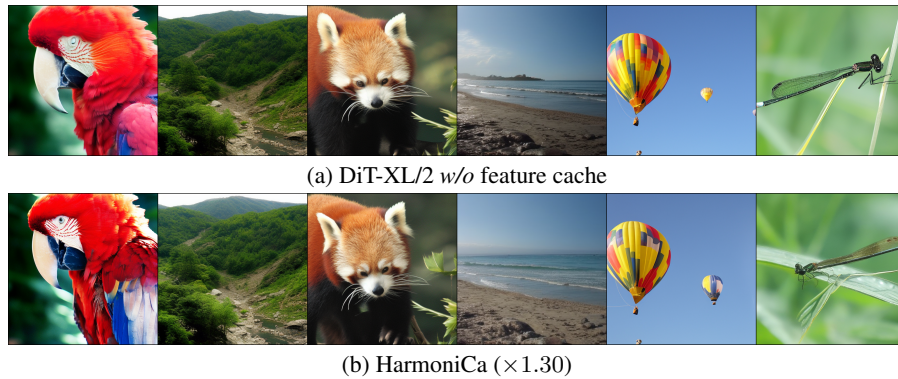


Figure C: Random samples from (a) non-accelerated and (b) accelerated DiT-XL/2 512×512 (Chen et al., 2023) with a 20-step DDIM sampler (Song et al., 2020a). The resolution of each sample is 512×512 .

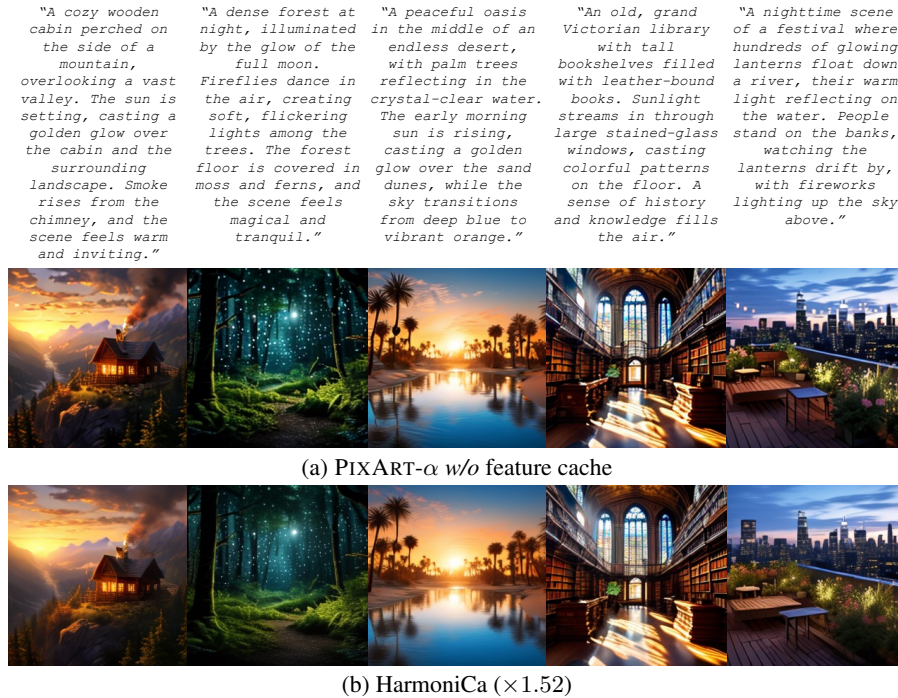


Figure D: Random samples from (a) non-accelerated and (b) accelerated PIXART- α 256×256 (Chen et al., 2023) with a 20-step DPM-Solver++ sampler (Lu et al., 2022b). The resolution of each sample is 256×256 . Text prompts are exhibited above the corresponding images

"A floating crystal palace high above the clouds, with intricate spires and towers made of transparent, glowing crystals. The sky is filled with radiant sunlight, and the clouds below reflect the palace's brilliance, creating a bright, cyberpunk night heavenly, magical scene."

"Two samurais clad in futuristic, neon-infused armor face off in a high-tech dojo. Their glowing katanas clash as electric sparks fly. The scene is set against a backdrop of towering city buildings and a sky."

"A massive dragon with shimmering scales glides over a dense, enchanted forest. Its wings create powerful gusts of wind, rustling the treetops below. The dragon's scales reflect the sunlight, creating a dazzling, majestic spectacle."

"In the depths of a dark, shadowy forest, a glowing portal of swirling blue and purple energy opens between ancient, twisted trees. A faint light emanates from the portal, casting an otherworldly glow on the forest floor covered in fallen leaves and mist."

(a) PIXART- α w/o feature cache(b) HarmoniCa ($\times 1.51$)

Figure E: Random samples from (a) non-accelerated and (b) accelerated PIXART- α 512×512 (Chen et al., 2023) with a 20-step DPM-Solver++ sampler (Lu et al., 2022b). The resolution of each sample is 512×512 .

"A medieval knight in full armor standing in a castle courtyard, holding a sword with both hands. His face is solemn as he prepares for battle, while the flags of the kingdom flutter behind him in the wind."

"A ballet dancer mid-pirouette on an empty stage, her elegant movements illuminated by a single spotlight. Her tutu swirls around her as she leaps gracefully through the air, capturing the essence of motion and grace."

"An ancient, majestic castle nestled atop a mountain peak, surrounded by swirling clouds, illuminated by golden sunlight. A dragon circles above, while knights stand guard below. The scene is full of magical realism, detailed stone walls, and elaborate banners flapping in the wind."



"A futuristic space station orbiting a colorful planet, surrounded by glowing stars and nebulae. Astronauts float near the station, with sleek spacecraft docking. The image captures the vastness and wonder of space, with intricate details on the station's metallic structure."

"A curious red fox exploring a snow-covered forest, its fur blending with the white landscape. Its sharp eyes scan the surroundings as it sniffs the ground, leaving delicate paw prints in the snow."

"A sleek, advanced city at dawn, with shimmering glass towers, floating gardens, and high-tech transportation systems. The sky is painted with pastel colors as the sun rises, casting a golden glow over the futuristic landscape."



(a) PIXART- α w/o feature cache



(b) HarmoniCa ($\times 1.51$)

Figure F: Random samples from (a) non-accelerated and (b) accelerated PIXART- α 1024×1024 (Chen et al., 2023) with a 20-step DPM-Solver++ sampler (Lu et al., 2022b). The resolution of each sample is 1024×1024 .

"Two colossal mechas, each covered in intricate armor plating and glowing power cores, engage in battle in the middle of a futuristic city. Skyscrapers crumble around them as they exchange powerful blows, and the energy radiating from their weapons lights up the night sky."

"A gargantuan sea creature with towering spines and glowing eyes rises from the ocean, water cascading off its massive form. Lightning illuminates the stormy sky as ships scramble to escape its wrath, emphasizing the creature's immense size and power."

"A colossal, ancient citadel made of shining marble and gold, perched atop the clouds. Massive towers and archways reach towards a sky filled with radiant sunlight, while a staircase of light descends from the heavens, hinting at the citadel's divine origins."



"A vast army of warriors clad in glistening armor charging across an icy battlefield under a stormy, dark sky. Blizzards rage around them, and the ground shakes as they clash with their enemies. The scene is filled with motion, energy, and the raw power of war."

"A majestic phoenix, its wings spread wide, emerges from a massive pillar of fire. The flames swirl around it in a dance of red, gold, and blue, while sparks and embers fill the air. Its form is both terrifying and beautiful, a symbol of rebirth and eternal power."

"A titanic clash between two massive, glowing deities in the sky, with thunderbolts and energy waves exploding around them. Below, mountains crumble and oceans churn as their power shakes the very fabric of reality, creating a breathtaking cosmic spectacle."



(a) PIXART- Σ w/o feature cache



(b) HarmoniCa ($\times 1.47$)

Figure G: Random samples from (a) non-accelerated and (b) accelerated PIXART- Σ 1024×1024 (Chen et al., 2024a) with a 20-step DPM-Solver++ sampler (Lu et al., 2022b). The resolution of each sample is 1024×1024 .

"Two samurais locked in a fierce duel under a cherry blossom tree, depicted in the traditional Japanese Ukiyo-e style. The bold outlines, flat colors, and exaggerated poses capture the intensity of the moment, while the delicate cherry blossoms fall gently around them."



"A peaceful alpine village nestled in the shadow of towering, snow-capped mountains, painted in a detailed realism oil painting style. The wooden houses have sloping roofs covered in snow, and smoke rises gently from their chimneys. The brushwork captures the texture of the wood and the soft shadows cast by the evening light."



"A studio photograph of an elegant Asian woman in a flowing silk dress. Her hair is styled in soft waves, and the smooth fabric of her dress reflects the studio lights gently. The high-definition shot focuses on the intricate textures of her skin and hair, as well as the subtle glint of light in her eyes."



(a) PIXART- Σ w/o feature cache

(b) HarmoniCa ($\times 1.51$)

Figure H: Random samples from (Left) non-accelerated and (Right) accelerated PIXART- Σ -2K (Chen et al., 2024a) with a 20-step DPM-Solver++ sampler (Lu et al., 2022b). The resolution of each sample is 2048×2048 .